JOURNAL OF MATERIALS SCIENCE 29 (1994) 4065–4069

Structure, stoichiometry and phase purity of strontium-doped lanthanum manganite powders

R. MILLINI*, M. F. GAGLIARDI, G. PIRO
Enitricerche S.p.A., Via F. Maritano 26, I-20097 San Donato Milanese (MI), Italy

Strontium-doped lanthanum manganite $La_{1-x}Sr_xMnO_3$ (LSM) is characterized by hexagonal–rhombohedral distorted perovskite-type structure, deriving from the ideal cubic symmetry through rotation of the $[MnO_6]$ octahedra around the ternary axis. The extent of distortion and unit cell volume depend on Sr content. The linear variation of the unit cell volume, observed in the compositional range $0.1 \leqslant x \leqslant 0.5$, can be effectively used for determining the stoichiometry of LSM. A procedure for the quantitative analysis of segregated impurities (La_2O_3 and Mn_3O_4) based on X-ray powder diffraction analysis, has also been developed.

1. Introduction

The electrical and mechanical properties of perovskite-type strontium-doped lanthanum manganite ($La_{1-x}Sr_xMnO_3$, hereafter indicated as LSM) make this material suitable for application as a cathode in solid oxide fuel cell (SOFC) technology. LSM-based cathodes are actually used for developing SOFCs in both tubular form (e.g. by Westinghouse) and flat plate concepts (e.g. by ABB, Siemens, ECN); for an overview see Grosz *et al.* [1].

The physico-chemical properties of LSM depend on the strontium fraction x which can vary in the range 0–0.70 [2]. Achievement of high electrical conductivity, high thermal and chemical stability, and chemical and mechanical compatibility with yttria stabilized zirconia (YSZ) electrolyte requires the stoichiometry of LSM to be carefully controlled. In particular, the electrical and mechanical properties of LSM-based cathodes are affected by the following:

(a) The distribution of strontium ions within the perovskite lattice, to which the distribution of lattice defects is related. A non-homogeneous distribution of Sr results in decreasing electrical conductivity.

(b) Impurities (usually arising from incompletely reacted materials), which constitute a barrier to the electrical conduction while reducing the mechanical stability of the cathode. Hydration of segregated La_2O_3 particles causes disintegration of sintered sample [3], while reaction of impurities with YSZ at the cathode–electrolyte interface produces non-conductive phases degrading the electrochemical properties of the cell [4].

This emphasizes the importance of finding effective methods for determining the real stoichiometry of LSM materials and for the quantitation of secondary phases present in the cathode powders.

In this paper, procedures for assessing LSM materials in terms of stoichiometry and phase purity, based on the X-ray powder diffraction technique, are presented and discussed.

2. Experimental procedure

2.1. Synthesis

LSM samples were prepared via an amorphous citrate process [5], starting from solutions containing the required concentration of metal acetates or nitrate and an excess of citric acid. The precursors, obtained by solvent evaporation via a Rotavapor or spray-drying, were finally calcined at 1373 K in air flow for 8 h.

Some samples were prepared by solid-state reaction at high temperature. Stoichiometric amounts of La_2O_3 (99.98% purity), $Sr(NO_3)_2$ (99.5% purity) and $MnCO_3$ (purity grade) were mechanically mixed, pressed into pellets and heated at 1473 K for 12 h. The thermal treatment was repeated after crushing, mixing and pelletizing the powders.

2.2. Characterization

Chemical analysis was performed by inductively coupled plasma atomic emission spectrometry (ICP-AES), using a Jobin Yvon 38 II Plus spectrophotometer. X-ray powder diffraction (XRD) patterns were recorded on a computer-controlled Philips diffractometer equipped with a pulse-height analyser. Data were collected stepwise in the $20 \leqslant 2\theta \leqslant 92°$ angular region, with 0.03° 2θ step size (2401 steps)

* To whom correspondence should be addressed.

0022–2461

and 20 s accumulation time; CuK_α radiation (λ = 0.154178 nm) was used. The diffractometer was calibrated by using Si (NBS No. 640) reference standard.

2.3. Structural analysis

Structural analysis of LSM materials was performed by full-profile fitting method. (Rietveld analysis [6, 7]. The software package WYRIET [8], a personal computer version of the DBW3.2S program [9] implemented with graphical routines, was used. The pseudo-Voigt function, with refinable Gaussian contribution, was used to describe the peak shape, while the angular dependence of the peak full width at half maximum (FWHM) was described by the equation of Caglioti *et al.* [10]. Background intensity was defined by a cubic polynomial with refinable coefficients. The calculated peak intensity was distributed over three FWHMs on either side of the peak centre. Refinement was performed by considering the contribution of both K_{α_1} and K_{α_2} radiation (2:1 intensity ratio) to the reflection profile. Starting values of unit cell parameters were determined by least-squares fit to the interplanar spacing of single strong reflections selected in the XRD pattern. Iteration was stopped when the shift/standard deviation ratio was less than 0.3 for all the parameters (normally after 20–25 iterations).

2.4. Quantitative phase analysis

La_2O_3 content was determined by the full-profile fitting method, taking advantage of the relation between weight fraction and Rietveld scale factor, as proposed by Hill and Howard [11]:

$$W_i = \frac{S_i M_i Z_i V_i}{\Sigma_j (S_j M_j Z_j V_j)} \quad (1)$$

where W_i is the weight fraction, S_i the Rietveld scale factor, M_i the formula weight, Z_i the number of formula units per unit cell and V_i the unit cell volume for the ith phase.

The minimum content of secondary phase detectable with this procedure depends on the nature of the phase and is defined by the concentration below which most of reflections are indistinguishable from the statistical background intensity. Below this value, the impurity content can be evaluated by extrapolation from calibration curves determined by simulation of the XRD pattern of a mixture of ith and jth phases with a weight ratio W_i/W_j. An arbitrary value is fixed for S_j, the value of S_i being derived by the equation [12]

$$S_i = S_j \left(\frac{W_i}{W_j}\right) \frac{M_j Z_j V_j}{M_i Z_i V_i} \quad (2)$$

where the symbols assume the meaning indicated for Equation 1. In practice one or more reflections were selected for each phase from calculated spectra, and the integrated intensity measured. The following reflections were used

La_2O_3–LSM:LSM: 0 1 2 ($2\theta = 22.9°$)

La_2O_3: 0 0 2 ($2\theta = 29.1°$) + 0 1 1/1 0 1 ($2\theta = 30.0°$)

Mn_3O_4–LSM: LSM: 2 0 2 ($2\theta = 40.0°$) + 0 0 6 ($2\theta = 40.5°$)

Mn_3O_4: 1 2 1 ($2\theta = 36.2°$) + 0 0 4 ($2\theta = 36.5°$)

The calibration curve were calculated for 0–5 wt % La_2O_3–LSM and 0–10 wt % Mn_3O_4–LSM by considering a fixed LSM stoichiometry ($x = 0.15$). The contents of La_2O_3 and Mn_3O_4 can be evaluated by the resulting equations:

$$\frac{I(La_2O_3)}{I(LSM)} = 11.594[La_2O_3] \text{ (wt \%)} \quad (3)$$

$$\frac{I(Mn_3O_4)}{I(LSM)} = 0.880[Mn_3O_4] \text{ (wt \%)} \quad (4)$$

3. Results and discussion

3.1. Crystal structure of LSM

The crystal structure of LSM with various Sr contents, was refined starting from data reported for $LaAlO_3$ [13], with La(Sr) on sites of symmetry 32 (0, 0, $\frac{1}{4}$), Mn on a ternary axis (0, 0, 0) and O on a binary axis (X, 0, $\frac{1}{4}$), R$\bar{3}$c space group (hexagonal axes). The results are listed in Table I; a typical final Rietveld plot is shown in Fig. 1. The structure of LSM (Fig. 2) is isomorphous with that of ABO_3 compounds with trivalent A and B metal ions having ionic radii in the ratio of about 2:1 [14]. Due to the hexagonal–rhombohedral distortion of the perovskite lattice, the La(Sr) coordination polyhedron deviates from the ideal 12-coordination, with three short, six middle and three long La(Sr)–O bond distances. In contrast, the coordination of Mn is perfectly octahedral (Table I).

The partial substitution of La by Sr results in significant variations of hexagonal unit cell parameters (a_h and c_h). The data obtained in the present investigation are slightly different from those reported by Hammouche *et al.* [15], especially for the c_h parameter (Fig. 3). However, in terms of unit cell volume V_h the agreement between the two sets of data is satisfactory (Fig. 3c). V_h remains practically constant up to $x = 0.1$ and decreases, following a Vegard-type law, for $x > 0.1$. The linear regression of data reported in Table I results in the equation

$$V_h = 355.99 - 21.188x \quad (5)$$

which is close to that computed from data reported by Hammouche *et al.* [15]

$$V_h = 356.82 - 24.036x \quad (6)$$

Equation 5 can be effectively used for determining the stoichiometry of LSM materials ($x > 0.1$).

With increasing Sr content the [La(Sr)O_{12}] coordination polyhedron moves towards the regular cubo-octahedral geometry (Table I), as indicated by the progressive reduction of lattice distortion. In the Mn–O bond distance decreases as a consequence of the increasing amount of Mn^{4+}.

TABLE I Crystal data (e.s.d. values in parentheses) for LSM samples with different Sr contents.

Sample	1	2	3	4	5	6
x^a	0	0.11	0.16	0.20	0.30	0.51
M_w	241.84	236.20	233.64	231.59	225.94	215.69
D (mg m^{-3})	6.82	6.67	6.60	6.57	6.44	6.23
a_h (nm)	0.552 80(1)	0.552 49(1)	0.552 26(1)	0.551 33(1)	0.549 16(2)	0.544 86(2)
c_h (nm)	1.334 04(3)	1.335 54(3)	1.335 66(3)	1.336 60(3)	1.337 92(4)	1.341 61(4)
V_h(nm^3)	0.353 05(1)	0.353 05(1)	0.352 79(1)	0.351 85(1)	0.349 42(2)	0.344 93(2)
x^b	–	0.14	0.16	0.20	0.31	0.52
X(O)	0.5489(8)	0.5458(8)	0.5446(8)	0.5430(9)	0.5353(9)	0.5185(9)
Mn–O (nm) 6 ×	0.1963(3)	0.1961(3)	0.1960(3)	0.1956(3)	0.1948(3)	0.1932(3)
La–O (nm) 3 ×	0.2496(5)	0.2509(5)	0.2515(5)	0.2518(5)	0.2552(5)	0.2624(5)
La–O (nm) 6 ×	0.2750(2)	0.2750(2)	0.2749(2)	0.2745(2)	0.2743(2)	0.2736(2)
La–O (nm) 3 ×	0.3032(3)	0.3015(3)	0.3008(3)	0.2992(3)	0.2940(3)	0.2825(3)
a_r (nm)	0.54736	0.54766	0.54762	0.54756	0.54719	0.54676
α_r (deg)	60.66	60.58	60.56	60.46	60.24	60.12
ω (deg)^c	9.89	9.28	9.12	8.26	5.63	3.86
t^d	0.956	0.965	0.969	0.973	0.981	0.997

[a] In $La_{1-x}Sr_xMnO_3$, from chemical analysis.
[b] In $La_{1-x}Sr_xMnO_3$, from Equation 5.
[c] Rotation-angle of the [MnO_6] octahedron. [10]; for an ideal cubic perovskite structure $\alpha_r = 60°$ and $\omega = 0°$
[d] Tolerance factor [17].

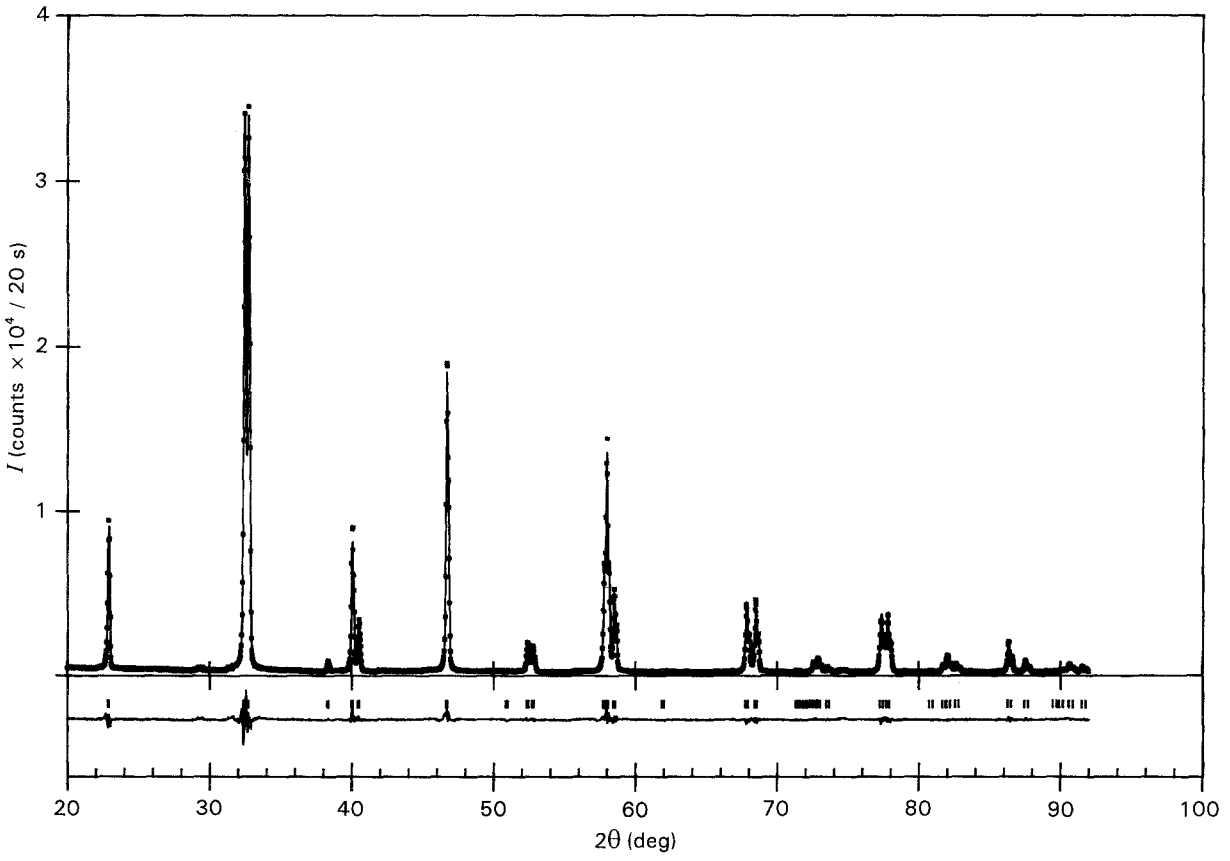

Figure 1 (■) Experimental and (——) calculated data and (below) difference trace of X-ray diffraction pattern of LSM (sample 4). Vertical bars indicate the positions of the Bragg reflections.

The deviation from ideal cubic symmetry may be rationalized by considering the rhombohedral unit cell parameters (a_r and α_r, derived from a_h and c_h according to the procedure reported in the International Tables of Crystallography). According to Morean *et al.* [15] the extent of hexagonal–rhombohedral distortion of the ABO_3 perovskite lattice, arising from rotation of [BO_6] octahedra around the ternary axis ([1 1 1] direction), is defined by the angle ω, [16].

The distortion of a perovskite lattice can also be described by the tolerance factor t defined by

$$t = \frac{r_A + r_O}{\sqrt{2}(r_B + r_O)} \quad (7)$$

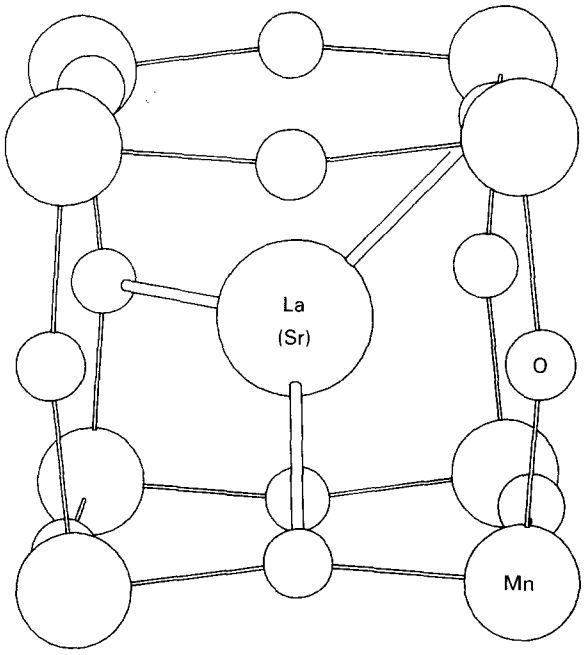

Figure 2 Representation of the distorted La(Sr) coordination polyhedron in the LSM structure. Mn–O bonds and the shortest La(Sr)–O interactions are shown.

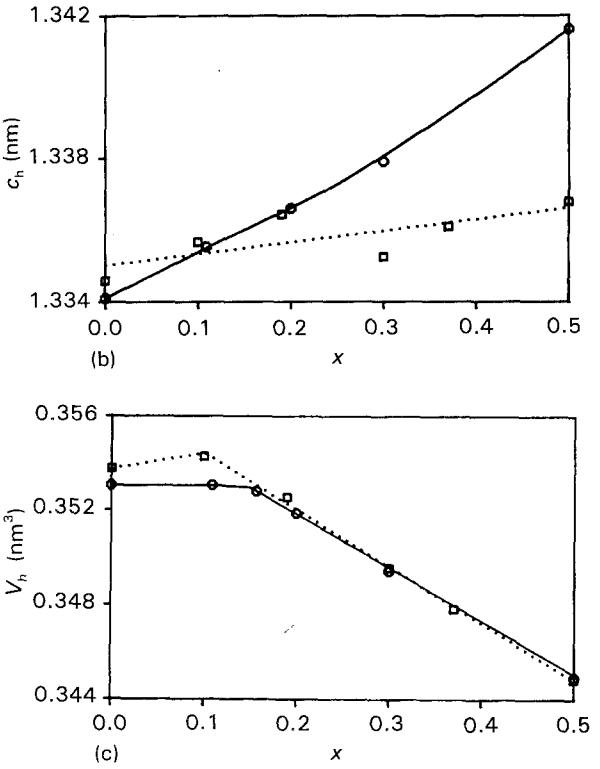

Figure 3 (○) Variations of (a) a_h, (b) c_h and (c) V_h of LSM as a function of Sr content x; (□) data reported by Hammouche *et al.* [15].

which assumes the value of 1 unit in the ideal perovskite structure and $t < 1$ in a rhombohedrally distorted lattice [17]. The ionic radii r_A and r_B were assumed equal to the weighted averages of values typical of single metal ions ($r_{La} = 0.136$ nm, $r_{Sr} = 0.144$ nm, $r^{3+}_{Mn} = 0.064$ nm, $r^{4+}_{Mn} = 0.053$ nm) and $r_O = 0.140$ nm [18].

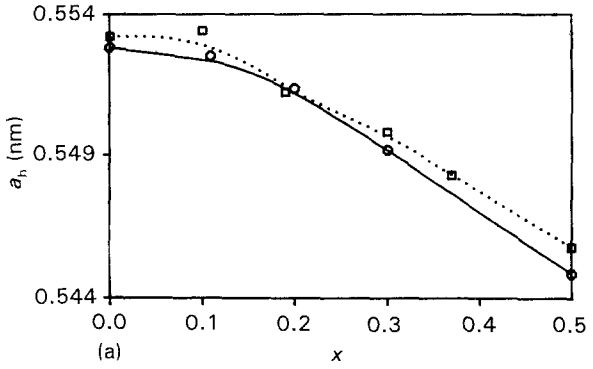

Rotation angles ω and tolerance factors t for samples 1–6 are reported in Table I. As the Sr content increases, ω decreases and t becomes closer to 1, indicating a progressive transition from rhombohedral symmetry towards the cubic perovskite lattice.

3.2. Phase purity

The purity of LSM materials is strictly dependent on the synthesis procedure. The early procedure, based on solid-state reaction among stoichiometric quantities of the corresponding metal oxides and/or car-

TABLE II Analytical and crystallographic data (e.s.d. value in parentheses) for LSM samples

Sample	Composition		a_h (nm)	c_h (nm)	V_h (nm^3)	x^a	La_2O_3 (wt %)		Mn_3O_4 (wt %)	
	La/Mn	Sr/Mn					C.A.[b]	XRD	C.A.[b]	XRD
7	0.89	0.19	0.552 02(2)	1.336 77(4)	0.352 77(4)	0.15	5.2	4.5(4.8[c])	–	–
8	0.81	0.22	0.551 31(4)	1.335 58(6)	0.351 55(7)	0.21	1.7	1.5(1.2[c])	–	–
9[d]	0.85	0.18	0.551 51(3)	1.334 36(4)	0.351 49(6)	0.20	4.7	4.1(4.0[c])	–	–
10	0.79	0.22	0.551 19(1)	1.335 42(4)	0.351 36(4)	0.22	–	0.7	–	–
11	0.81	0.21	0.551 42(3)	1.335 93(4)	0.351 79(4)	0.20	–	1.1	–	–
12[d]	0.69	0.18	0.551 81(3)	1.337 25(5)	0.352 63(5)	0.16	–	–	8.1	8.4
13	0.79	0.11	0.552 26(1)	1.336 02(3)	0.352 88(3)	0.14	–	–	2.3	2.1
14	0.77	0.21	0.551 34(1)	1.336 03(2)	0.351 71(2)	0.20	–	–	–	–
15	0.77	0.21	0.551 42(1)	1.335 71(2)	0.351 73(2)	0.20	–	–	–	–
16	0.81	0.21	0.551 31(1)	1.335 50(2)	0.351 53(2)	0.21	–	–	–	–

[a] In $La_{1-x}Sr_xMnO_3$, from Equation 5.
[b] Chemical analysis.
[c] Determined by full-profile fitting analysis (Equation 1).
[d] By solid-state synthesis.

bonates, has been almost completely replaced by the so-called "wet chemical methods". The latter generally lead to higher interdispersion of metal ions and higher reactivity of the amorphous precursor, assuring enhanced purity of the final product together with a better control of powder morphology. In spite of the effectiveness of wet chemical methods, it is not unusual to obtain LSM powders containing significant amounts of secondary phases (mostly La_2O_3 and Mn_3O_4). Quantitation of the above phases via full-profile fitting of XRD patterns (Equation 1) was successfully achieved only in the case of La_2O_3–LSM mixtures with more than 1 % wt La_2O_3 (samples 7–9, Table II). Attempts to refine the XRD patterns of Mn_3O_4–LSM binary mixtures failed, probably because of line convolution. Evaluation of low La_2O_3 contents and/or Mn_3O_4 content requires using the calibration curves derived by Equations 3 and 4; the results, reported in Table II, are in good agreement with those derived from both chemical analysis and the full-profile fitting method.

4. Conclusions

LSM has a hexagonal–rhombohedral structure arising from a distortion of the perovskite structure through rotation of the $[MnO_6]$ octahedra around the ternary axis. The degree of distortion decreases as the strontium content increases. X-ray diffraction analysis constitutes a powerful tool for qualifying LSM powders in terms of their stoichiometry and purity.

Acknowledgements

This work was supported by SNAM S.p.A. (San Donato Milanese). The authors are grateful to Dr F. Bazzano for elemental analysis and to Dr G. Perego for helpful discussions.

References

1. F. GROSZ, P. ZEGERS, S. C. SINGHAL and O. YAMAMOTO (eds), Proceedings of 2nd International Symposium on Solid Oxide Fuel Cells, Athens, July 1991 (Office for Official Publication of the European Communities, Luxembourg, 1991).
2. G. H. JONKER, *Physica* **22** (1956) 707.
3. E. BERGSMARK, S. FURUSETH, O. DYRLIE, T. NORBY and P. KOFSTAD, in Proceedings of 2nd International Symposium on Solid Oxide Fuel Cells, edited by F. Grosz, P. Zegers, S. C. Singhal and O. Yamamoto (Office for Official Publications of the European Community, Luxembourg, 1991) p. 473.
4. O. YAMAMOTO, Y. TAKEDA, R. KANNO and M. NODA, *Solid State Ionics* **22** (1987) 241.
5. P. COURTY, B. DELMON, C. MARCILLY and A. SUGIER, Belgian Patent 735476 (1969).
6. H. M. RIETVELD, *Acta Crystallogr.* **22** (1967) 151.
7. *Idem, J. Appl. Cryst.* **2** (1969) 65.
8. J. SCHNEIDER, in Proceedings of International Workshop of the Rietveld Method, Petten (The Netherlands), 1989, Abstract B17.
9. B. D. WILES and R. A. YOUNG, *J. Appl. Cryst.* **14** (1981) 149.
10. G. CAGLIOTI, A. PAOLETTI and F. P. RICCI, *Nucl. Instrum.* **3** (1958) 223.
11. R. J. HILL and C. J. HOWARD, *J. Appl. Cryst. Allogr.* **20** (1987) 467.
12. R. J. HILL, *Powder Diffrcn* **6** (1991) 74.
13. B. DERIGHETTI, J. E. DRUMHELLER, F. LAVES, K. A. MÜLLER and F. WALDNER, *Acta Crystallogr.* **18** (1965) 557.
14. O. MÜLLER and R. ROY, "The Major Ternary Structural Families" (Springer, Berlin, 1974) p. 184.
15. A. HAMMOUCHE, E. SIEBERT and A. HAMMOU, *Mater. Res. Bull.* **24** (1989) 367.
16. J. M. MOREAU, C. MICHEL, R. GERSON and W. J. JAMES, *Acta Crystallogr.* **B26** (1970) 1425.
17. A. J. JACOBSON, B. C. TOFIELD and B. E. F. FENDER, *ibid.* **B28** (1972) 956.
18. R. D. SHANNON, *ibid.* **A32** (1976) 751.

Received 26 November 1992
and accepted 28 January 1994